PROCEEDINGS OF THE ROYAL SOCIETY A

Proc. R. Soc. A (2008) **464**, 1057–1077
doi:10.1098/rspa.2007.0140
Published online 7 February 2008

Spatio-temporal information in an artificial olfactory mucosa

By Manuel A. Sánchez-Montañés[1], Julian W. Gardner[2] and Timothy C. Pearce[3,*]

[1]*Escuela Politécnica Superior, Universidad Autónoma de Madrid, Madrid 28049, Spain*
[2]*School of Engineering, University of Warwick, Coventry CV4 7AL, UK*
[3]*Department of Engineering, University of Leicester, Leicester LE1 7RH, UK*

Deploying chemosensor arrays in close proximity to stationary phases imposes stimulus-dependent spatio-temporal dynamics on their response and leads to improvements in complex odour discrimination. These spatio-temporal dynamics need to be taken into account explicitly when considering the detection performance of this new odour sensing technology, termed an artificial olfactory mucosa. For this purpose, we develop here a new measure of spatio-temporal information that combined with an analytical model of the artificial mucosa, chemosensor and noise dynamics completely characterizes the discrimination capability of the system. This spatio-temporal information measure allows us to quantify the contribution of both space and time to discrimination performance and may be used as part of optimization studies or calculated directly from an artificial mucosa output. Our formal analysis shows that exploiting both space and time in the mucosa response always outperforms the use of space alone and is further demonstrated by comparing the spatial versus spatio-temporal information content of mucosa experimental data. Together, the combination of the spatio-temporal information measure and the analytical model can be applied to extract the general principles of the artificial mucosa design as well as to optimize the physical and operating parameters that determine discrimination performance.

Keywords: machine olfaction; information theory; artificial olfactory mucosa

1. Introduction

Chemical sensor arrays for odour analysis, which form the basis of electronic noses, typically rely upon a wide diversity of chemical sensors, each ideally tuned differentially to individual chemical compounds (for an overview, see Pearce *et al.* 2003). The detection capability of a chemical sensor array for complex (multicomponent) odour analysis is determined by both sensor noise and the degree to which response properties can be made stimulus specific and diverse across the array (Pearce & Sánchez-Montañés 2003). One way of improving detection performance in these systems is to make use of temporal

* Author for correspondence (t.c.pearce@le.ac.uk).

Received 21 July 2007
Accepted 3 January 2008

information arising from sensor dynamics. This potentially increases the diversity of array responses, thereby contributing more information regarding the stimulus (Llobet *et al.* 1997).

A second method of exploiting time in these systems is to introduce spatio-temporal dynamics into the stimulus itself, which in turn imposes complex dynamics on the sensor response. These dynamics can be similarly exploited for the purposes of improved detection as long as they can be made stimulus specific. We have shown these principles at work in a fabricated artificial mucosa device that discriminates complex odours reliably (Gardner *et al.* 2007). In general, such artificial mucosa sensor systems are able to produce very rich spatio-temporal responses on account of the dynamics of odour transportation combined with the sensor dynamics. Since the spatial segregation of odours within the artificial mucosa and the sensor kinetics can both depend upon the specific molecular species, the combined system has potential for a highly capable multicomponent chemical analysis system. In the olfactory pathway of mammals, odour delivery is a complex process of turbulent flow through the external nares and odorant uptake by the olfactory mucosa, which mediates transport to olfactory receptor sites. This process imposes both spatial and temporal aspects on the chemicals delivered to the receptor sheet, which is likely to be relevant to the processing of chemosensory information (for a review, see Schoenfeld & Cleland 2006). Specifically, there is evidence that similar stimulus-specific spatial segregation of odorants is also exploited in the mammalian olfactory system as a mechanism for odour discrimination (Kent *et al.* 1996). These aspects lead us to believe that the principles of combined spatial segregation of odorants and distributed chemosensors with broad tunings are a highly effective approach to complex odour analysis.

Exploiting these mechanisms for the purposes of odour discrimination is not straightforward, since the total detection capability of the system depends upon the combined dynamics, the sensor tunings and their noise properties. There are many fundamental questions that such a system poses. For instance, how much better could we identify different stimuli in such a system that uses spatio-temporal information compared with one that does not use temporal information? To address this issue, we conduct here a formal analysis of the combined artificial mucosa architecture that leads to a closed-form equation for spatio-temporal information which defines its detection performance and the effect of each of the key parameters in the system. This information theoretic measure may be used as part of optimization schemes in the design of artifical olfactory systems to improve complex odour discrimination.

2. Distributed chemosensor and artificial mucosa dynamics

(*a*) *Odour dynamics*

The artificial olfactory mucosa concept exploits chemosensors distributed within or in sufficiently close proximity to stationary phases (figure 1) by imposing complex spatio-temporal dynamics on the stimulus and chemosensor array responses through the principle of selective partitioning of compounds existing within a mixture (complex odours). Three mechanisms for complex odour discrimination exist in this device, which we should take into account in any comprehensive performance analysis.

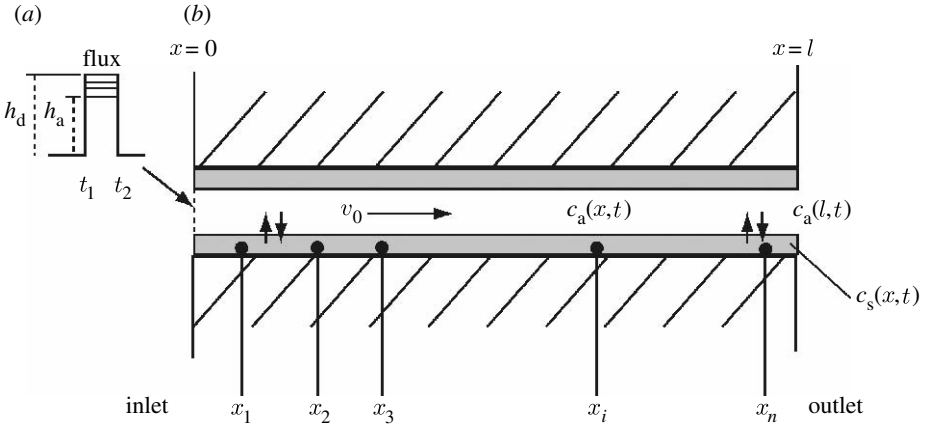

Figure 1. Schematic of the artificial olfactory mucosa. (*a*) A rectangular pulse of complex odour, comprising many individual compounds a, b, etc. of concentrations c_a, c_b, etc. is injected into a carrier gas travelling through (*b*) a microchannel at velocity v_0. The interior surface of the microchannel is coated with a stationary phase material into which odours partition differently according to their affinity. These affinities determine the relative time each ligand type spends in the stationary phase compared with the mobile phase, which determines in equilibrium the velocity of transportation along the channel with respect to the carrier velocity. Each chemosensor (depicted by filled circles) can be placed at a different position, x_i and may have independent tunings to the different compounds. We denote the output of each sensor i as $y_i(t)$ in continuous time t or $y_i(m)$ in discrete (sampled) time.

(i) The chemosensor array itself (discounting the effect of the stationary phase for the moment) may have a wide spectrum of broad 'tunings' to the different volatile compounds of interest. A given sensor i at position x_i possesses a fixed tuning or specificity to the analytes under investigation out of the set of possible tunings. As a result, a spatial fingerprint of a particular complex odour will be generated across the array that is typically stimulus specific and may be used as part of the pattern recognition scheme for odour discrimination (Pearce *et al.* 2003). In this case, we do not consider the role of time explicitly, but rather the magnitudes of the responses across the array.

(ii) The injection of the complex odour pulse into a mobile carrier phase, inside the mucosa, moving at velocity v_0 (figure 1) alongside a stationary phase, leads to differential partitioning of components within a complex odour causing odour components to segregate in space within the artificial mucosa ('chromatographic effect'; Purnell 1962). Depending upon the affinity of each analyte to the stationary phase coating of the artificial mucosa, in the steady state, each compound will be found within the stationary and mobile (carrier) phases in a fixed ratio according to the odour-specific partition coefficient $k'_j = (c_{sj}/c_j)$, where c_{sj} and c_j are the analyte concentrations in the stationary and mobile phases, respectively. This retards the progress of the pulse for that compound through the mucosa, which provides a second mechanism for odour discrimination. Thus depending upon their location in the mucosa, each sensor will receive a particular sequence of single or subsets of components within a complex mixture over time as a function of the stimulus. We will

later see that this sequence gives rise to a temporal fingerprint in the chemosensor response that is highly sensitive to the presence of odour components or compounds.

(iii) The chemosensor dynamics themselves can also depend upon the compounds present in the mixture, leading to an additional dimension of temporal variation that can be exploited for the purposes of discrimination.

By conducting an information theoretic analysis, we have previously quantified the effect of the first mechanism on discrimination performance in chemical sensor arrays, which was able to account for both noise properties in the sensors and the tunings to a set of odour compounds in determining detection capability (Sánchez-Montañés & Pearce 2001; Pearce & Sánchez-Montañés 2003). However, that analysis ignored the temporal or transient properties of the sensor signals, which form the basis for the second and third mechanisms for discrimination discussed above.

In this paper, we conduct a detailed dynamical and information theoretic analysis, which accounts for all three mechanisms for odour discrimination in an artificial mucosa. We begin with an analysis of the second mechanism of discrimination by modelling the physical segregation of ligands within the artifical olfactory mucosa. After this, we will treat the sensor dynamics themselves as either first- or second-order dynamical processes, which are combined with the mucosa dynamics model to derive a numerical scheme for predicting the sensor output response within the mucosa.

The motivation for this combined model is threefold. First, through the development of such models we can better understand the dynamics of the combined system and their relationship to the key system parameters. Second, although we fit the model to data obtained for two compounds, it is, however, general and so can predict responses across a continuum of the key parameters involved. Third, the development of this model allows us to study hypothetical mucosa designs, which may be used to extract general design principles, or may be used as part of a general optimization scheme. We will also see that in the end this performance measure does not depend upon these models explicitly but can be computed directly from artificial mucosa data.

Our analysis proceeds in two steps. First, we develop a model of the dynamics of responses of chemosensors distributed within an artificial mucosa that is fitted to experimental data. Second, we derive and apply a new measure of spatio-temporal information to the chemosensor responses that provides a limit to the detection performance of the system. We then use this theory to (a) prove formally that exploiting both space and time in the mucosa response always outperforms using space alone, and (b) demonstrate this performance advantage by comparing the spatial versus spatio-temporal information content of artificial mucosa experimental data.

(*b*) *Spatio-temporal odour dynamics*

We first consider the dynamics of chemical compound migration through the artificial mucosa (figure 1). Positive (negative) pressure is created at the inlet (outlet) of the system to produce a carrier flow into which a pulse of chemical

is introduced. For a fixed concentration s_j (molar concentration) of stimulus compound j at the inlet, the amount of material introduced into the microchannel per unit time (flux) is $h_j = s_j A v_0$ (mol s^{-1}), where A is the cross-sectional area inside the microchannel itself, which is $A = (z_0 - 2d)^2$, given that z_0 is the square cross-sectional thickness, for a given film thickness d, and v_0 is the velocity of the carrier flow. For low carrier velocities, such that phase equilibrium occurs, the velocity of a particular ligand through the microchannel is fixed and depends upon the mass distribution coefficient, k_j, which is related to the partition coefficient, k'_j, through $k_j = k'_j q$, where q is the phase ratio of volumes in the stationary and mobile phases, respectively. The velocity of analyte j through the microchannel is then simply given by $v_j = v_0/(1 + k_j)$ (Purnell 1962).

From the diffusion–convection equation, Golay (1958) considered the separation of chemicals within circular and square cross-section gas–liquid capillary chromatographic columns and derived a partial differential equation for local concentration of compound j, $c_j(x', t)$, at time t and position x' within the microchannel, which we apply here as follows:

$$D'_j \frac{\partial^2 c_j}{\partial x'^2} = \frac{\partial c_j}{\partial t}, \tag{2.1}$$

where the change of variables $x' = x - (v_0 t/(1 + k_j))$ has been used to simplify the expression, and x' is now the displacement with respect to a moving coordinate system travelling at velocity $v_0/(1 + k_j)$, this being the average velocity of the pulse through the artificial mucosa. D'_j is the effective diffusion coefficient that combines the effects of the geometry of the channel (in this case square cross-section), non-uniform Poiseuille flow and static and dynamic diffusion within both the mobile and stationary phases given by

$$D'_j = \frac{D_{mj}}{(1 + k_j)} + \frac{2\left(1 + 9k_j + 51k_j^2/2\right)}{105(1 + k_j)^3} \frac{v_0^2 z_0^2}{D_{mj}} + \frac{k_j^2}{3(1 + k_j)^3} \frac{v_0^2 z_0^2}{D_{sj}}, \tag{2.2}$$

where D_{mj} and D_{sj} are the true diffusion coefficients of compound j in the mobile and stationary phases, respectively.

The heat–diffusion partial differential equation of equation (2.1) has the well-known solution for its impulse response in the form of the Green's function (Crank 1975)

$$c_j(x', t) = \frac{1}{2\sqrt{D'_j \pi t}} \exp\left(-\frac{x'^2}{4D'_j t}\right). \tag{2.3}$$

The impulse response of the artificial mucosa in the original coordinate system to a Dirac delta function of compound j is therefore a travelling Gaussian, moving at constant velocity v_j, which depends upon the carrier flow velocity, v_0, and the mass distribution coefficient, k_j, and disperses with characteristic length $\sqrt{2D'_j t}$ over time. In the case where the analyte is introduced as a square pulse extending in time between t_1 (onset) and t_2 (offset; a 'sniff'), the solution is given by convolving the impulse response of equation (2.3) with the stimulus pulse of temporal width $T = t_2 - t_1$ (figure 1*a*, left). After convolving with the stimulus and returning to the original coordinate system x, we obtain after some algebra

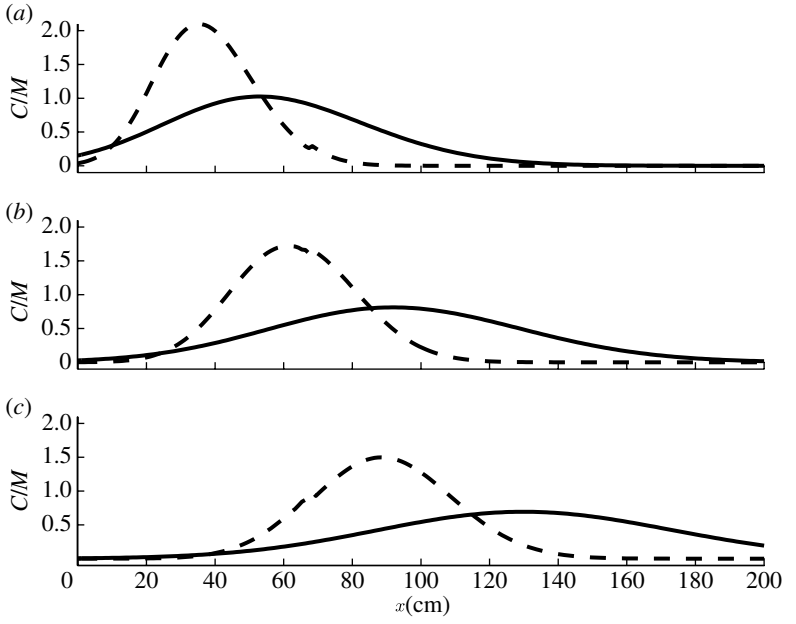

Figure 2. Numerical solution of equation (2.4) for the separation of two odour components (a, solid line; b, dashed line) within the artificial olfactory mucosa ((*a*) $t=10$ s, (*b*) $t=15$ s and (*c*) $t=20$ s). $v_0=15\ \mathrm{cm\ s^{-1}}$, mass distribution coefficients $k_\mathrm{a}=1$ and $k_\mathrm{b}=2$, and effective diffusion coefficients $D'_\mathrm{a}=50\ \mathrm{cm^2\ s^{-1}}$ and $D'_\mathrm{b}=10\ \mathrm{cm^2\ s^{-1}}$. Pulse duration $T=5$ s, stimuli concentration $s_\mathrm{a}=s_\mathrm{b}=1\ \mathrm{mol\ cm^3}$.

(see appendix A)

$$c_j(x,t)=\frac{s_j(1+k_j)}{2}\left[\mathrm{erf}\left(\frac{v_j u-x}{2\sqrt{D'_j u}}\right)+\exp\left(\frac{v_j x}{D'_j}\right)\mathrm{erf}\left(\frac{v_j u+x}{2\sqrt{D'_j u}}\right)\right]_{u=\max(0,t-T)}^{u=t}, \tag{2.4}$$

where erf is the error function.

Figure 2 shows the progress through the microchannel of two compounds a and b injected simultaneously at the inlet at time zero (pulse duration $T=5$ s). We see a separation between the two compounds which increases over time and depends directly upon the difference in partition coefficients. In both cases, it is the dispersion of the mobile phase in air that determines the degree of overlap and this depends upon the effective diffusion coefficient D'. As the spatio-temporal dynamics can be made stimulus specific, these provide additional information about the stimulus as a means for discrimination (mechanism (ii), §2*a*).

(*c*) *Sensor dynamics*

For the purposes of quantifying spatio-temporal information in the artificial mucosa, we now consider a phenomenological model of the carbon black/polymer chemosensors used in the mucosa when placed both inside and outside the mucosa device. Full fabrication and sensor details for the artificial mucosa that we model are provided elsewhere (Gardner *et al.* 2007). However, briefly, the

artificial mucosa was constructed by mounting discrete polymer/carbon black composite chemoresistive sensors (40 devices of 10 different composites) on a printed circuit board base sealed with two different polyester lids (with and without stationary phase coating, which we refer to here as the coated and uncoated mucosa) within which a serpentine microchannel was machined. Once sealed, this composite structure was injected with poly-chloro-*p*-xylylene (parylene C), as the absorbent stationary phase material, deposited using a commercial evaporation technique (PDS 2010 Lab-coater 2, Specialty Coating Systems, Indianapolis, USA). Each sensor chip was $2.5\times4.0\,\mathrm{mm}^2$ in size and comprised a pair of thin coplanar gold electrodes on a SiO_2/Si substrate with an electrode length of 1.0 mm and an inter-electrode gap of 75 μm. We are not interested here in the mechanistic details or physical principles of the sensor chemical interactions *per se.* Rather, we require a sufficiently accurate operational description of the sensor response dynamics and noise properties during exposure to mixtures to allow us to quantify the total detection capability of the system.

Establishing linearity in the sensors over time and varying concentrations are critical if we are interested in the performance of the mucosa for being able to estimate the concentration of individual compounds existing within a mixture—i.e. the inverse problem. Linearity here refers to (a) approximately linear scaling of the sensor response waveform with increasing concentration, and (b) linear superposition over time, such that the temporal response to the mixture is at all times the linear addition of the response to the individual compounds. Both principles are essential if we are to solve easily the inverse problem using linear processing methods and apply Fisher information, as we discuss later.

We have separately shown experimentally that the sensors are linear up to relatively high concentrations of pure alcohols (Koickal *et al.* 2007).

In terms of superposition over time, we created binary mixtures of toluene (compound a) and ethanol (compound b) and exposed these to the sensor array within the mucosa to assess linearity to mixtures. For this purpose, we keep the total flow constant. Since the tubes and delivery pressures are not identical, we expect a weighted linear summation in the sensor response where the weights do not sum *a priori* to 1. We compared the weighted linear superposition, $w_\mathrm{a}y_\mathrm{a}(m)+w_\mathrm{b}y_\mathrm{b}(m)$, of the individual responses at each time step m, $y_\mathrm{a}(m)$ and $y_\mathrm{b}(m)$, for toluene and ethanol, respectively, with the sensor response to the mixture, $y_{\mathrm{a}+\mathrm{b}}(m)$ (figure 3*a*). The plots show the sensor responses to the mixture (solid) compared with the weighted linear mixture of time series (circles) for the individual compounds (where w are fitted parameters, $w_\mathrm{a}=0.2$ and $w_\mathrm{b}=0.74$). We observe that sensors with different polymer coatings at different locations within the channel clearly produce varied temporal responses arising from the third mechanisms of discrimination discussed previously. For sensors with different carbon black/polymer coatings (for details, see Gardner *et al.* 2007) responding to identical stimuli, we are then able to predict the mixture responses using the same w parameters in each case (figure 3*a*,*b*).

Note that even though the sensors are at very different locations within the microchannel, the data of figure 3 show no significant time difference in their onset transient times (latencies). This is because for this experiment a relatively high flow rate was used, giving insufficient time for partitioning with the

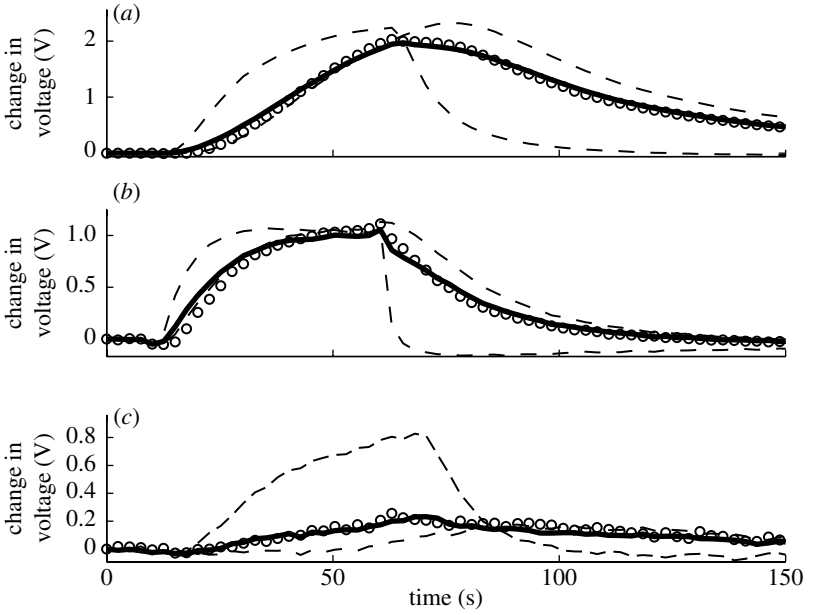

Figure 3. Demonstration of linear superposition of actual chemosensor responses inside the artificial mucosa for two compounds (toluene and ethanol) mixed at their respective saturated vapour pressures (SVPs) before delivery into the artificial mucosa. Dashed plots show the actual sensor response to the individual compounds at SVP, whereas the solid plot is the actual response to the mixture. The predicted linear superposition (circles) is shown for comparison over time. Sensor materials: (*a*) sensor 20, poly-chloro-*p*-xylylene; (*b*) sensor 3, poly(ethylene glycol); and (*c*) sensor 39, PSF. The w parameters of the weighted summation were fitted to sensor 20 and then used to test the linearity of the other sensors across the array.

stationary phase and little time for dispersion (i.e. diffusional spreading) in the microchannel itself ($v_0 = 50\ \mathrm{cm\ s^{-1}}$). However, the flow rate in itself makes little difference to the principle of superposition in the sensors and so separation is not required for establishing this fact.

Our results clearly show that the predicted temporal response to the mixture agrees well with the linear superposition of the individual compounds, demonstrating linearity across time for the compounds tested. Hence, we conclude that the sensors behave sufficiently linearly over time to low–moderate concentrations of analyte such as are found in the artificial mucosa and real-world olfactory problems.

We next require a dynamical model of the sensor response. We proceed by constructing phenomenological first- and second-order dynamical models and fitting them against responses of different sensors with carbon black/polymer coatings to controlled step inputs outside the mucosa device (figure 4*a*,*c*). For the second-order model, the sensor response, $y(t)$, is described by the weighted summation of two first-order processes, which may have different time constants λ_1 and λ_2, where these time constants may be stimulus dependent, accounting for the third discrimination mechanism discussed earlier. Depending upon the sensor coating (carbon black/polymer), we found that either a first- or second-order model was sufficient to describe accurately different sensor responses.

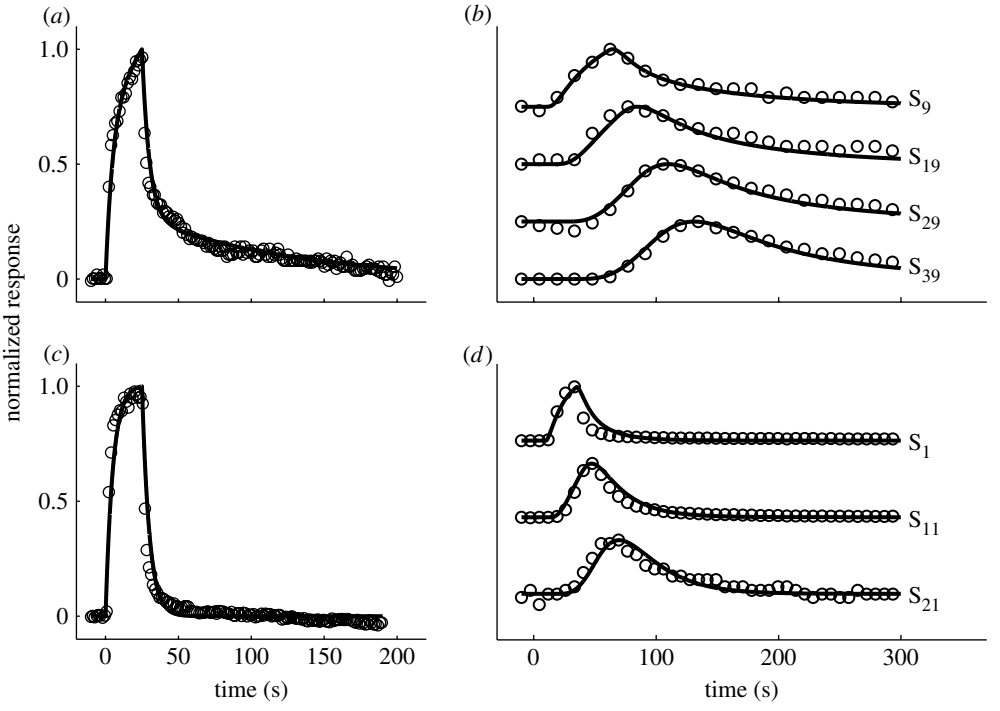

Figure 4. Fit and prediction of actual sensor responses outside and within the artificial mucosa. (*a*) A second-order model is fitted to carbon black/polymer PSF sensor response data responding to a square pulse of ethanol at SVP outside the microchannel (pulse duration $T=25$ s). Fitted parameters: time constants, $\lambda_1=5$ s and $\lambda_2=100$ s; sensor gain, $g_1/g_2=523.0$. (*b*) An identical second-order model is now convolved with equation (2.4) and partially fitted (D' and k) to carbon black/polymer PSF sensor responses to a rectangular pulse of ethanol (at SVP at the inlet, pulse duration $T=50$ s) at four different positions inside the microchannel (S_9, 30 cm; S_{19}, 99 cm; S_{29}, 168 cm; S_{39}, 224 cm). Carrier flow velocity, $v_0=5$ cm s^{-1}. Fitted parameters: mass distribution coefficient, $k=0.82$; effective diffusion coefficient, $D'=49.0$ cm^2 s^{-1}. (*c*) A first-order model is fitted to carbon black/polymer PEVA sensor responses to a rectangular pulse of ethanol at SVP outside the microchannel (pulse duration $T=25$ s). Fitted parameters: time constant, $\lambda=5$ s. (*d*) An identical first-order model is now convolved with equation (2.4) using mucosa parameters identical to (*b*) and the predicted response is compared with the data from carbon black/polymer PEVA sensor responses to a rectangular pulse of ethanol (at SVP at the inlet, pulse duration $T=25$ s) at three different positions inside the microchannel (S_1, 1 cm; S_{11}, 57 cm; S_{21}, 126 cm). Each response magnitude in (*b*,*d*) is normalized to unity.

(*d*) *Combined mucosa model dynamics*

In order to test the accuracy of the combined first- and second-order chemosensor and microchannel dynamical models, we convolved the two numerically in order to generate the time dependence of sensor responses at different locations resulting from the travelling stimulus pulse, as shown in figure 4*b*,*d*. With increasing sensor distance from the inlet, the latency of the onset transient clearly increases, directly resulting from the travel time of the stimulus pulse through the mucosa. This latency is also observed to be stimulus dependent, depending upon the mass distribution constant k, while the broadening in the response with increasing distance depends upon the effective diffusion coefficient D'.

We checked the combined sensor and microchannel model in two steps, the result of which is shown in figure 4*b*,*d*. First, we computed the parameters that fit the isolated poly(sulfane) (PSF) sensor data (outside the mucosa) in response to a square pulse (figure 4*a*). Then, equation (2.4) was used with the known sensor positions of all PSF sensors and carrier flow velocity within the mucosa device, and was fitted to the PSF chemosensor responses simultaneously, by varying the global parameters k and D' (figure 4*b*). Second, similarly for another chemosensor type, PEVA, we first fitted a first-order model (figure 4*c*) to data taken outside the mucosa device and then used the fitted time constant, λ, to predict its response in the mucosa device operating under the same conditions and with the input similar to that used in figure 4*b*. The model behaviour using independently fitted parameters is shown to provide an accurate prediction of the sensor time-series data, as shown in figure 4*d*. Thus, we conclude that our combined model provides a sufficiently accurate description of the artificial mucosa response in terms of all the key physical parameters, for the purposes of optimization and configuration testing.

An important property of the combined model and hence the artificial mucosa itself is linearity in terms of the relationship between low–moderate analyte concentrations of presented mixtures and the corresponding chemosensor responses. This makes the processing of sensor responses straightforward in this system and makes the classification, segmentation and estimation of chemical stimuli straightforward using linear statistical and data processing methods. Moreover, linearity is important for calculating Fisher information, which we will see later greatly simplifies the analysis.

(*e*) *Noise dynamics*

Since the mucosa performance is strictly limited by the chemosensor noise, we require a phenomenological model of this to perform any system characterization. For this reason, we consider additive noise to give a sensor response $y_i(m) = \overline{y_i}(m) + n_i(m)$, where $\overline{y_i}(m)$ is the mean sensor response at time step m of a sampling process over many trials to the same identical mixture. The noise process n_i for each sensor i is then approximated by a linear first-order autoregressive (AR) time-series model, such that

$$n_i(m+1) = \gamma_i n_i(m) + \sigma_i \sqrt{1-\gamma_i^2}\,\xi_i(m), \tag{2.5}$$

with $m \in [1, M-1]$, where M is the total number of consecutive sensor samples. Here, $n_i(1)$ is modelled as a Gaussian random variable of zero mean and variance σ_i^2. The coefficients γ_i and σ_i may depend on each sensor and $\xi_i(m)$ is an independent and identically distributed (IID) Gaussian variable of unit variance and zero mean, which is sampled independently for each time step and each sensor. This implies that n_i also has zero mean, variance σ_i^2 and an autocovariance given by

$$\langle n_i(m) n_i(m+d) \rangle = \sigma_i^2 \gamma_i^{|d|}. \tag{2.6}$$

The correlation time in the noise is then $\tau_i = \Delta t/(1-\gamma_i)$, where Δt is the sample period and has variance σ_i^2 that is directly proportional to the total power in the noise spectrum. The parameters γ_i and σ were fitted for each sensor using the AR

forward–backward algorithm (Marple 1980)—the result of one of these operations for sensor PSF can be seen in figure 5*d* ($\gamma = 0.58$, $\sigma = 6.6 \times 10^{-3}$).

Using vectorial notation for the whole sequence $[n_i(1), \ldots, n_i(M)]^{\mathrm{T}}$, the noise vector $\boldsymbol{n}_i$ is a multivariate Gaussian process with M components, zero mean and (auto) covariance matrix $\boldsymbol{N}_i$ given by

$$\boldsymbol{N}_i(u, v) = \sigma_i^2 \gamma_i^{|u-v|}. \tag{2.7}$$

Henceforth, we will use parentheses to indicate the element of the vector (m) or matrix (u, v) to avoid confusion with subscripts.

To verify the noise model, we took typical sensor responses during repeat trials and averaged the response over trials, to estimate $\overline{y_i}(m)$ at each time step, as shown in figure 5*a*. As an estimate of the noise process, we then subtracted the individual sensor response for a single trial $y_i(m)$ from the mean response at each time step to obtain an estimate of the instantaneous noise process (figure 5*b*). We see that the model and sensor noise processes are qualitatively similar (cf. figure 5*b*,*d*). We further compared the sensor and model noise processes in the frequency domain, giving a similar $1/f^2$ dependence.

The independence of the noise across the array is also important in determining the overall noise performance of the system. Correlated common-mode noise (due either to sensors or associated instrumentation) has less effect than independent noise in terms of corrupting sensor responses and can usually be easily removed. Even so, we empirically tested the cross-correlation of the noise time series between chemosensors in the artificial mucosa while responding to the same stimulus (figure 5*e*). We find that there is little common-mode noise across the array in our system since the zero time-lag cross-correlation peaks are relatively low. We will later use this fact to greatly simplify the analysis of the information content.

3. Quantification of spatio-temporal information in chemosensor arrays

We next derive a novel spatio-temporal information measure based upon Fisher information. In previous work, we have demonstrated how Fisher information can be used to quantify the performance of chemical sensor arrays for the complex odour analysis (Sánchez-Montañés & Pearce 2001; Pearce & Sánchez-Montañés 2003). Briefly, the Fisher information matrix (FIM), $\boldsymbol{F}$, is a square and symmetric matrix of $s \times s$ components, where s is the number of individual compounds whose concentrations we wish to estimate. The FIM contains all necessary components to characterize the tuning, noise and detection performance in the array. In order to calculate $\boldsymbol{F}$, we should first calculate the individual FIMs for each sensor i

$$\boldsymbol{F}_i = \int p(\boldsymbol{Y}_i|\boldsymbol{c}) \left(\frac{\partial \ln p(\boldsymbol{Y}_i|\boldsymbol{c})}{\partial \boldsymbol{c}} \right) \left(\frac{\partial \ln p(\boldsymbol{Y}_i|\boldsymbol{c})}{\partial \boldsymbol{c}} \right)^{\mathrm{T}} \mathrm{d}^M \boldsymbol{Y}_i, \tag{3.1}$$

where $\boldsymbol{Y}_i$ is the response of sensor i and $\boldsymbol{c}$ is a vector with the concentrations of the s compounds existing within a mixture (odour space). Equation (3.1) is general in that the sensor response $\boldsymbol{Y}$ may either represent a time-independent scalar or a time-series vector (of dimension M). The probability distribution $p(\boldsymbol{Y}_i|\boldsymbol{c})$ represents the noisy response of the sensor to a given mixture with

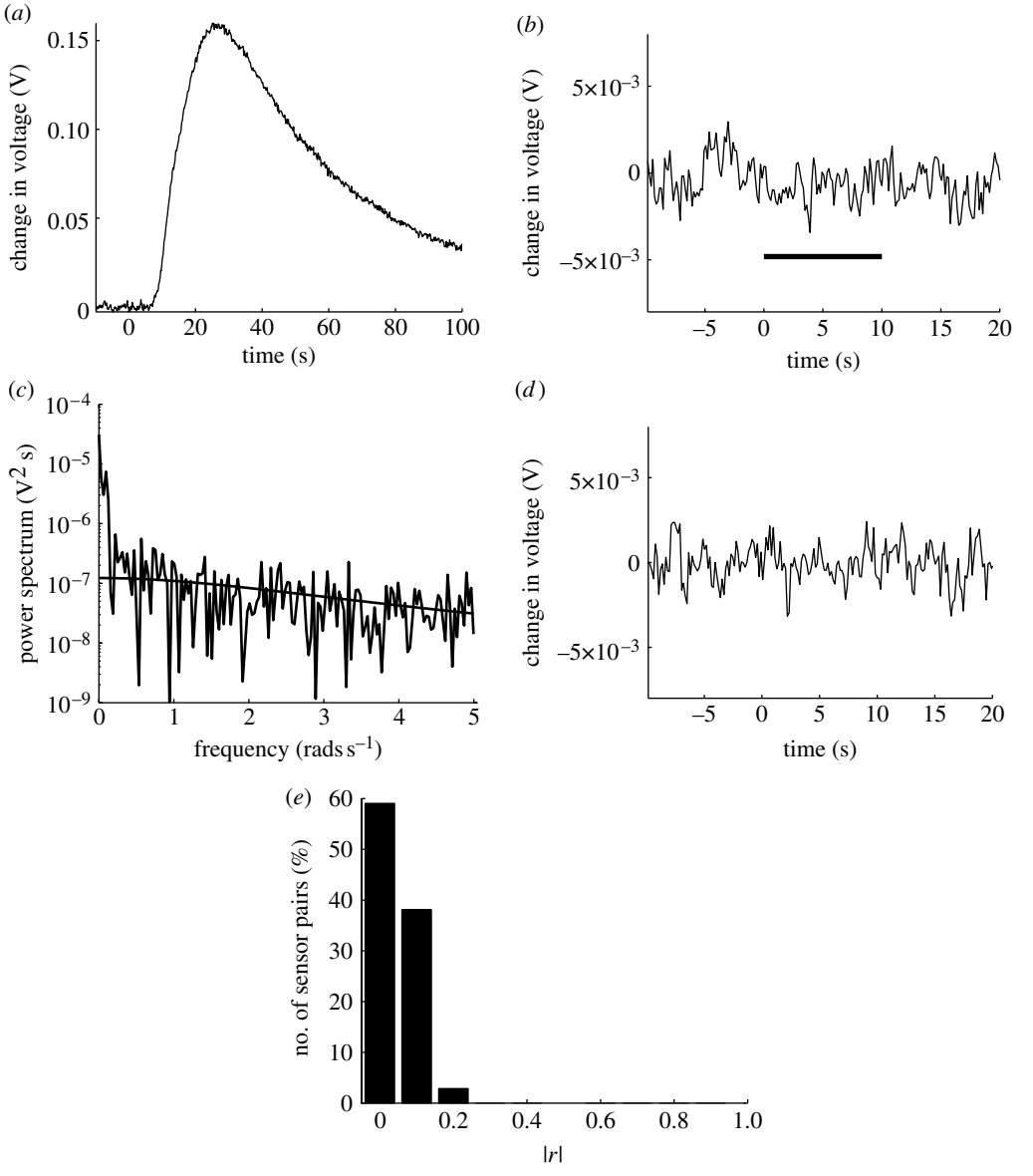

Figure 5. The sensor input channel noise described and fitted by an AR process. (*a*) Mean PSF chemosensor response from three repeat trials to toluene and ethanol mixed in air at their respective SVPs (pulse duration $T=10$ s). (*b*) The instantaneous fluctuation between the actual sensor response for one of the trials and the mean. The bar indicates the stimulus onset and offset. (*c*) The noise spectrum of the modelled AR noise process alongside that of the PSF sensor. (*d*) The time series of the AR process described by equation (2.5) for comparison. (*e*) Time-zero peak in the cross-correlation across all pairs of sensors within the array.

concentration vector, $\boldsymbol{c}$. In the case where the noise in each sensor is independent over all time (there is no common-mode noise), as we demonstrated is approximately the case for our array, then the total FIM for the array, $\boldsymbol{F}$, is equal to the summation of the individual matrices for each sensor, $\boldsymbol{F}_i$.

The usefulness of Fisher information is given by the important property that the best square error across all unbiased techniques that use the noisy array responses to estimate the stimulus is (for discussion, see Sánchez-Montañés & Pearce 2001)

$$\epsilon^2 = \mathrm{trace}(\boldsymbol{F}^{-1}). \tag{3.2}$$

Moreover, the FIM $\boldsymbol{F}$ is closely related to the discrimination capability of the system, which is why we consider it in this context. For instance, it can be demonstrated that in a two-alternative forced choice (2-afc) discrimination task between two stimuli (i.e. the system has to determine which of the two possible complex odours $\boldsymbol{c}_1$ and $\boldsymbol{c}_2$ is being presented), the optimal probability of error, $P(\epsilon)$, that can be achieved with linear sensors is

$$P(\epsilon) = \frac{1}{2}\left[1 - \mathrm{erf}\left(\frac{\sqrt{\lambda}}{2}\right)\right], \tag{3.3}$$

with $\lambda \equiv (1/2)\Delta\boldsymbol{c}^{\mathrm{T}}\boldsymbol{F}\Delta\boldsymbol{c}$ and $\Delta\boldsymbol{c} \equiv \boldsymbol{c}_2 - \boldsymbol{c}_1$. Hence, we may use the Fisher information to estimate directly the likelihood of error in discriminating between any two mixtures presented to the system.

In our previous work, we have discussed how to calculate in practice the Fisher information when the temporal patterns of the responses of the individual sensors are not taken into account (corresponding to the first mechanism for discrimination identified in §2*a*). Here we extend and calculate the Fisher information for the spatio-temporal case, explicitly including the role of time in the responses. The first step is to model the noise in the sensors, which will estimate $p(\boldsymbol{Y}_i|\boldsymbol{c})$. We first describe the noise model verified for the sensors in §2*e* using vectorial notation. Let us first define $\boldsymbol{Y}_{i;\boldsymbol{c}}$, which is a vector of M components (number of consecutive samples of the sensor), as the noisy temporal response (time series) of sensor i to stimulus $\boldsymbol{c}$. As before, we will consider sensors with additive noise

$$\boldsymbol{Y}_{i;\boldsymbol{c}} = \overline{\boldsymbol{Y}}_{i;\boldsymbol{c}} + \boldsymbol{n}_i, \tag{3.4}$$

where $\overline{\boldsymbol{Y}}_{i;\boldsymbol{c}}$ is the mean sensor response time series averaged over many trials to the same identical mixture $\boldsymbol{c}$, and $\boldsymbol{n}_i$ is a noisy time series that corrupts the individual sensor response (see §2*e*).

(*a*) *Spatio-temporal Fisher information*

The average response of a linear sensor i to a mixture $\boldsymbol{c}$ is given by (ignoring the constant sensor baseline)

$$\overline{\boldsymbol{Y}}_{i;\boldsymbol{c}} = \sum_j c_j \boldsymbol{A}_i^j, \tag{3.5}$$

where $\boldsymbol{A}_i^j$ is the average response time series of sensor i to a unit of concentration of single compound j. Equation (3.5) implies that the sensor response is linear to increasing concentration (within some reasonable limit) and to mixtures which we demonstrated for the artificial mucosa to realistic concentrations in §2*c*.

Using the result obtained in §2*e* that $\boldsymbol{Y}_{i;\boldsymbol{c}}$ is a Gaussian vector with covariance matrix $\boldsymbol{N}_i$, together with equation (3.1), it is straightforward to demonstrate that

$$\boldsymbol{F}_i(u, v) = (\boldsymbol{A}_i^u)\boldsymbol{N}_i^{-1}(\boldsymbol{A}_i^v)^{\mathrm{T}}, \tag{3.6}$$

where u and v are matrix indices. Using this result together with equation (2.5) as well as the fact that the chemosensors are causal ($A_i(1,k)=0$), we can derive after some algebra the following result:

$$\boldsymbol{F}_i(u,v) = \frac{1}{\sigma_i^2(1-\gamma_i^2)} \sum_{m=2}^{M} \boldsymbol{B}_i^u(m)\boldsymbol{B}_i^v(m), \tag{3.7}$$

with $\boldsymbol{B}_i^j(m) \equiv \boldsymbol{A}_i^j(m) - \gamma_i \boldsymbol{A}_i^j(m-1)$. This important equation represents the spatio-temporal Fisher information of a noisy sensor within an array and can be directly applied to the sensor data as we show later.

(*b*) *Purely spatial Fisher information*

It is interesting to quantify the improvement in spatio-temporal information compared with the information carried by the sensor responses when no explicit temporal information is considered. To perform this, we consider the contribution of the first mechanism and the second and third mechanisms combined. For example, when the output of each sensor that is used in subsequent signal processing is simply the average response to the stimulus

$$y_{i;\boldsymbol{c}} = \frac{1}{M} \sum_{m=1}^{M} \boldsymbol{Y}_{i;\boldsymbol{c}}(m), \tag{3.8}$$

then it is easy to demonstrate that this response is a Gaussian variable with average $\boldsymbol{a}_i^{\mathrm{T}}\boldsymbol{c}$, where

$$a_i(u) \equiv \frac{1}{M} \sum_{m=1}^{M} \boldsymbol{A}_i(m,u). \tag{3.9}$$

The variance of $y_{i;\boldsymbol{c}}$ can be also calculated as

$$\sigma_i^2(y_{i;\boldsymbol{c}}) = \frac{\sigma_i^2}{(1-\gamma_i)^2 M^2}\left[M\left(1-\gamma_i^2\right) - 2\gamma_i(1-\gamma_i)\right]. \tag{3.10}$$

Then, the individual Fisher information matrices are given by (Sánchez-Montañés & Pearce 2001)

$$\boldsymbol{F}_i = \frac{1}{\sigma_i^2(y_{i;\boldsymbol{c}})} \boldsymbol{a}_i \cdot \boldsymbol{a}_i^{\mathrm{T}}, \tag{3.11}$$

which may be compared with the spatio-temporal case in equation (3.7).

The Fisher information results arrived at in §3*a*,*b* may be combined with the spatio-temporal and noise models to assess and optimize the detection performance of different operating conditions and artificial mucosa designs. However, equations (3.7) and (3.11) for quantifying the spatio-temporal and spatial information, respectively, may also be applied directly to an artificial olfactory mucosa output to assess detection performance and compare the contributions of the different discrimination mechanisms introduced in §2*a*. We will later demonstrate the application of these equations to the mucosa sensor output in two different discrimination problems of varying difficulty (§4).

(*c*) *Spatio-temporal information is greater than spatial information in the artificial olfactory mucosa*

Now we demonstrate that the microchannel's spatio-temporal information is always greater or equal to purely spatial information, for any number of sensors independent of the number of components in the odour.

Let us call $\boldsymbol{Y}^*$ the vector formed by the concatenation of the individual sequences of sensor responses $\boldsymbol{Y}_i$. That is,

$$\boldsymbol{Y}^* \equiv \left[\boldsymbol{Y}_1^{\mathrm{T}}, \boldsymbol{Y}_2^{\mathrm{T}}, \ldots\right]^{\mathrm{T}}. \tag{3.12}$$

The task is then to estimate $\boldsymbol{c}$ from the spatio-temporal responses $\boldsymbol{Y}^*$. In the purely spatial case, the task is estimating $\boldsymbol{c}$ from $g(\boldsymbol{Y}^*)$, where the function g represents the extraction of the spatial information, which can be a linear operation (e.g. signal averaging) or nonlinear (e.g. maximum response).

Zamir (1998) shows that the FIM of a random variable $\boldsymbol{Y}^*$, and the FIM of a function of that variable, $g(\boldsymbol{Y}^*)$, always satisfies

$$\boldsymbol{F}(\boldsymbol{Y}^*|\boldsymbol{c}) - \boldsymbol{F}(g(\boldsymbol{Y}^*)|\boldsymbol{c}) \geq 0, \tag{3.13}$$

where the inequality represents that the difference matrix is positive semidefinite. Furthermore, Bhatia (2007) shows that if $\boldsymbol{A}$ and $\boldsymbol{B}$ are positive definite and $\boldsymbol{A}-\boldsymbol{B}\geq 0$, then $\boldsymbol{A}^{-1}-\boldsymbol{B}^{-1}\leq 0$. Using this, and the fact that for well-posed problems (i.e. the amount of information in the sensors is sufficient to estimate $\boldsymbol{c}$) the FIMs are positive definite, we obtain

$$\boldsymbol{F}^{-1}(\boldsymbol{Y}^*|\boldsymbol{c}) - \boldsymbol{F}^{-1}(g(\boldsymbol{Y}^*)|\boldsymbol{c}) \leq 0. \tag{3.14}$$

Now, applying the trace operator to this equation and using the property that it is linear, we obtain

$$\mathrm{trace}(\boldsymbol{F}^{-1}(\boldsymbol{Y}^*|\boldsymbol{c})) \leq \mathrm{trace}(\boldsymbol{F}^{-1}(g(\boldsymbol{Y}^*)|\boldsymbol{c})). \tag{3.15}$$

Using equation (3.2), we find that the optimal error bounds in the estimation of $\boldsymbol{c}$ satisfy

$$\epsilon^2_{\mathrm{sp-temp}} \leq \epsilon^2_{\mathrm{sp}}, \tag{3.16}$$

demonstrating the required result.

4. Results

(*a*) *Spatio-temporal and spatial Fisher information in a simple pure odour detection task*

We first considered the simplest class of problem for the artificial olfactory mucosa. In this case, two distinct pure compounds, ethanol and toluene, were introduced as a rectangular pulse into the microchannel (for details, see Gardner *et al.* 2007) and sensor responses recorded. We previously showed that this was a trivial task to solve by the artificial mucosa. In order to compare the contribution of spatial and temporal information for this task, we applied equations (3.7) and (3.11) to the mucosa output, which proceeded in a number of steps. First, each sensor time series $\boldsymbol{Y}$ was filtered, which was then used to estimate the parameters of the AR model, σ_i and γ_i of equation (2.5) using the AR forward–backward algorithm (Marple 1980). These parameters were then used in equations (3.7), (3.10) and (3.11) to construct FIMs for each sensor, which were summed to form

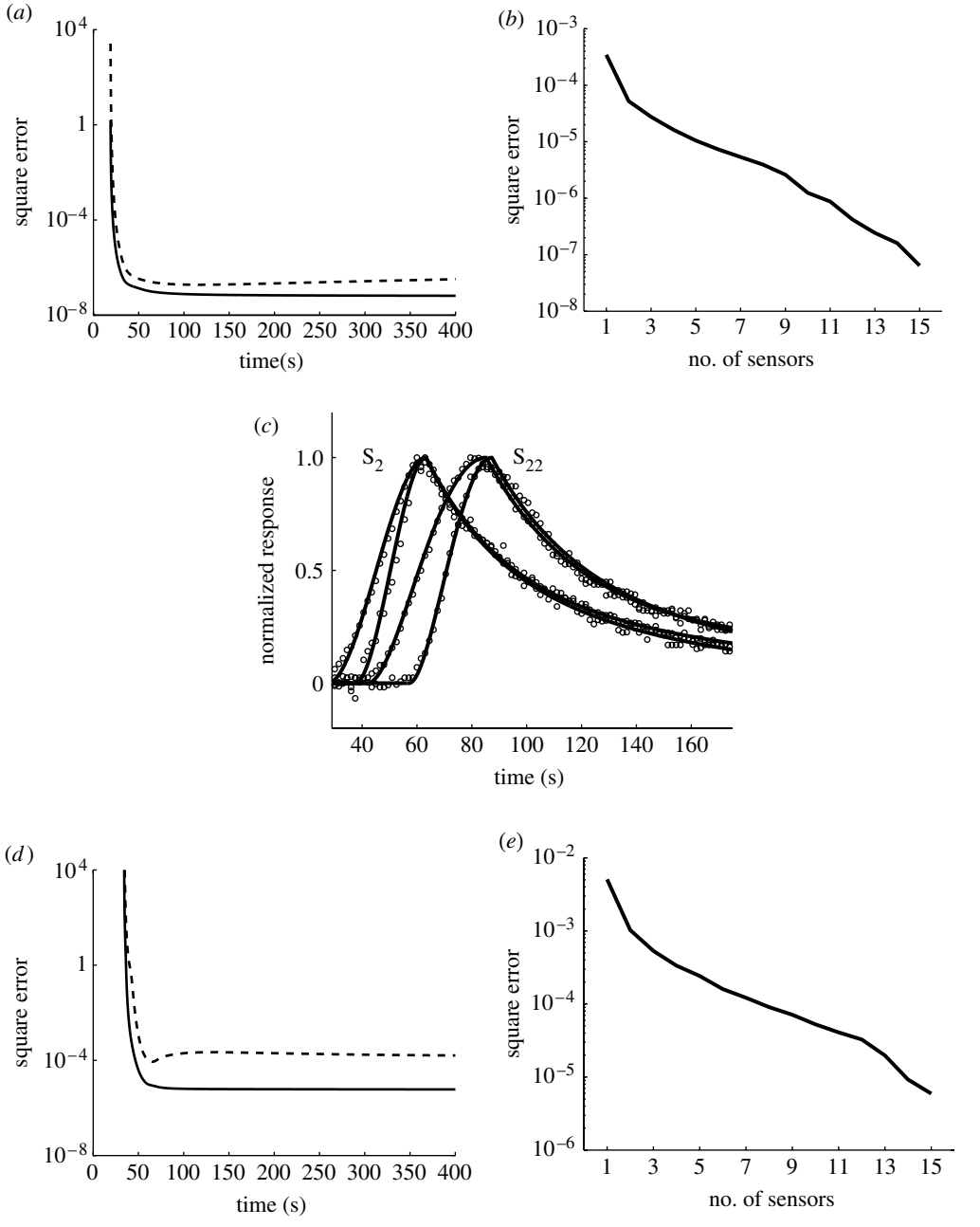

Figure 6. (*Caption opposite.*)

F leading directly to the optimal square error, calculated directly using equation (3.2). This process was repeated using different time-series lengths in order to characterize the square error detection performance over time.

The result of this procedure is shown in figure 6*a*. We see that the detection error of the system, which is initially infinite since only noise signals are available, reduces dramatically within the first 30 s as the pure odour enters

Figure 6. (*Opposite.*) Improvement in detection performance using spatio-temporal information. (*a*) Optimal square error in the estimation of the individual concentrations in mixtures of toluene and ethanol, as a function of the sampling time and using all of the 15 available sensors. Solid line, optimal square error, $\epsilon^2_{\mathrm{sp-temp}}$, when the spatial and temporal information in the sensor array is taken into account; dashed line, optimal square error, ϵ^2_{sp}, when only the spatial information is taken into account. (*b*) Best error using spatio-temporal information as a function of the number of sensors, toluene versus ethanol experiment. (*c*) Examples of two normalized sensor time series (S_2 and S_{22}) fitted by a second-order dynamical model in response to peppermint alone and to peppermint–vanilla mixture. (*d*) Optimal square error in the estimation of the pure and mixed stimulus of peppermint and peppermint–vanilla mixture, as a function of the sampling time and using all the 15 available sensors. Solid line, $\epsilon^2_{\mathrm{sp-temp}}$; dashed line, ϵ^2_{sp}. (*e*) Best error using spatio-temporal information as a function of the number of sensors for the peppermint versus peppermint–vanilla mixture experiment.

the microchannel and elicits sensor responses. The detection error quickly approaches some asymptoptic value $\epsilon^2_{\mathrm{sp-temp}}$ (for the spatio-temporal case), which represents the limit in overall performance of the mucosa in estimating the stimulus once all sensors have responded and the stimulus has left the microchannel. Importantly, we observe that the expected square error when using spatio-temporal information is always smaller than that error when only spatial information is considered.

In order to investigate how much spatio-temporal information improves as the number of sensors increases for this relatively simple task (arbitrary mixtures of the two pure odours, toluene and ethanol), we calculated the optimal error for each of the 32 767 sets of sensors that can be generated out of our 15 available sensors. Figure 6*b* shows that the best error using spatio-temporal information reduces by orders of magnitude as the number of sensors increases, demonstrating the importance of sensor array diversity in the artificial olfactory mucosa. We also investigated how much improved the spatio-temporal information is with respect to pure spatial information by calculating the ratio of the two optimal estimation errors ϵ^2_{sp} and $\epsilon^2_{\mathrm{sp-temp}}$ for all the 32 767 sets of sensors that can be generated (table 1). Specifically, for each possible subset of sensors, we have performed analogous calculations to those shown in figure 6*a*, and then computed the ratio of the minima of the two curves. Table 1 shows the resulting range of ratios for a given number of sensors. When using all the 15 available sensors in the array, the ratio of the two square errors is 3.0. The relatively small improvement is due to the fact that, in this case, the detection task is trivially solved using spatial information alone (the first discrimination mechanism) and only a few sensors. Thus, the system is overspecified for the task.

For configurations with only one sensor, the ratio is always infinite since it is impossible to estimate the concentrations of the individual compounds from the average response of only one sensor, a task which on the other hand is possible to address when the temporal information is also considered (table 1). For small numbers of sensors, the improvement in the performance of the system based on spatio-temporal information can be of several orders of magnitude, revealing that an artificial mucosa optimally designed for exploiting temporal features can dramatically increase the detection performance as well as reduce the number of total sensors required to solve a particular detection problem.

Table 1. Improvement in detection performance using spatio-temporal compared with spatial information for the toluene versus ethanol experiment. (Range of the ratio of errors of spatial information only to spatio-temporal information (ϵ^2_{sp}: $\epsilon^2_{\mathrm{sp-temp}}$) for all the possible configurations that can be generated out of 15 sensors.)

no. of sensors	ratio	no. of sensors	ratio
1	∞	9	1.9–27
2	1.9–2100	10	2.0–25
3	1.9–390	11	2.0–20
4	1.9–180	12	2.1–7.6
5	1.9–140	13	2.6–5.4
6	1.9–84	14	2.7–3.5
7	1.9–52	15	3.0
8	1.9–38		

(*b*) *Spatio-temporal and spatial Fisher information in a mixture detection task*

We next chose a more challenging detection task for the artificial mucosa, which was to present separately a pure compound (peppermint) alongside the same compound with an additional second component (vanilla). As one of the stimuli is a multicomponent odour, this is a more challenging discrimination task as we found in Gardner *et al.* (2007). Figure 6*c* shows the filtered responses of two example sensors within the mucosa responding to these two stimuli. Clearly, some temporal information that is stimulus specific exists in the responses (evidence of the second and third discrimination mechanisms).

As before, we calculated the time dependence of the square error using both space and time compared with space alone for this new task (figure 6*d*). We again observe that the error for the spatio-temporal case is always lower than that when the spatial information is considered alone. Moreover, owing to the fact that the magnitudes of the responses vary less between the stimulus classes, in this case, the temporal component makes far more contribution to reducing the asymptoptic error of the system. The ratio of the two optimal estimation errors using the 15 available sensors is 15.0 (table 2), which translates to approximately one order of magnitude error reduction. This represents a substantial per-formance advantage over traditional chemical sensor arrays, exploiting only the first and third discrimination mechanisms. Finally, figure 6*e* shows as in the toluene/ethanol experiment that the best error using spatio-temporal information reduces by orders of magnitude as the number of sensors increases.

5. Conclusions

We have presented a comprehensive performance analysis of a new complex odour detection technology, referred to as the artificial olfactory mucosa. We have shown, both experimentally and theoretically, that deploying chemical sensor arrays within the stationary phase materials provides a performance advantage over the classical electronic nose approach of controlling odour

Table 2. Improvement in detection performance using spatio-temporal compared with spatial information for the peppermint versus peppermint–vanilla mixture experiment. (Range of the ratio of errors of spatial information only to spatio-temporal information ($\epsilon^2_{\mathrm{sp}} : \epsilon^2_{\mathrm{sp-temp}}$) for all the possible configurations that can be generated out of 15 available sensors.)

no. of sensors	ratio	no. of sensors	ratio
1	∞	9	4.2–61
2	2.2–1400	10	5.5–59
3	2.3–530	11	7.0–38
4	2.5–470	12	8.5–30
5	2.7–290	13	9.8–23
6	2.8–250	14	14–19
7	3.2–110	15	15
8	3.5–92		

delivery across the whole array as a homogeneous pulse. The performance advantage in this system is obtained by exploiting all three mechanisms for discrimination we have identified, rather than a subset as in the classical approach. As we have seen, the addition of stationary phase materials introduces spatio-temporal dynamics into the odour delivery process that can be made stimulus specific, potentially adding more information about odour concentrations and composition. Using stationary phases in this way will also allow us to optimize sensor positions independently depending upon their preferred tunings so that key compounds of interest can be detected within a time frame of interest. Our analysis has also identified the linear operation of this combined mucosa. This important property means that odour classification, segmentation and estimation can proceed using linear statistical and other data processing techniques, vastly simplifying the signal analysis.

The combined model of mucosa, sensor and noise dynamics alongside the novel spatio-temporal information measure we have developed allows us to perform a comprehensive performance analysis. We have seen how the spatio-temporal information measure may be applied directly to an artificial mucosa output in order to assess the contribution of the different discrimination mechanisms to detection performance over time. Moreover, the theory can also be used to extract design principles for the artificial mucosa in terms of all the key operational parameters that affect their detection performance. Finally, the combined theory may be used to design optimal decoders of the mucosa output for odour classification, segmentation and estimation which is future work. We believe that the artificial mucosa approach to complex odour analysis and the underlying theory presented here will support a new generation of complex odour detection devices with improved performance.

We are grateful to Forest Su Tan and James Covington for building the physical implementation of the artificial olfactory mucosa. We also acknowledge the support of the Royal Society via a Joint European Research Project (to T.C.P. and M.A.S.-M.) and Engineering and Physical Sciences Research Council (to T.C.P. and J.W.G.). M.A.S.-M. was also supported by MEC (grant BFU2006-07902/BFI) and CAM (PRICIT 5-SEM-0255-2006).

Appendix A

Here we proceed to calculate the stimulus concentration across the microchannel for a rectangular pulse injected from $t=0$ to T. From equation (2.3) and the definition of x', $(x'=x-vt)$ with $v=(v_0/(1+k))$, the Green's function is given by

$$G(x,t') = \frac{1}{2\sqrt{D'\pi t'}}\exp\left(-\frac{(x-vt')^2}{4D't'}\right).$$

Then the molar concentration of the stimulus across the microchannel, for $t\in[0,T]$, is

$$c(x,t) = sv_0\int_0^t G(x,t-t')\mathrm{d}t',$$

whereas the molar concentration for $t>T$ is given by

$$c(x,t) = sv_0\int_0^T G(x,t-t')\mathrm{d}t'.$$

Thus, in general,

$$c(x,t) = sv_0\int_0^{\min(t,T)} G(x,t-t')\mathrm{d}t'.$$

Performing a change of coordinates $u\equiv t-t'$, we obtain

$$\begin{aligned} c(x,t) &= sv_0\int_{\max(0,t-T)}^{t} G(x,u)\mathrm{d}u \\ &= \frac{sv_0}{2}\int_{\max(0,t-T)}^{t}\frac{1}{\sqrt{D'\pi u}}\exp\left(-\frac{(x-vu)^2}{4D'u}\right)\mathrm{d}u. \end{aligned}$$

Let us consider the error function, $\mathrm{erf}(z)\equiv(2/\sqrt{\pi})\int_0^z \mathrm{e}^{-w^2}\mathrm{d}w$. It is easy to check by directly computing the derivative that

$$\frac{1}{v}\frac{\mathrm{d}}{\mathrm{d}u}\left[\mathrm{erf}\left(\frac{vu-x}{2\sqrt{D'u}}\right)+\exp\left(\frac{vx}{D'}\right)\mathrm{erf}\left(\frac{vu+x}{2\sqrt{D'u}}\right)\right] = \frac{1}{\sqrt{D'\pi u}}\exp\left(-\frac{(x-vu)^2}{4D'u}\right).$$

Using this fact, we obtain the required result

$$c(x,t) = \frac{s(1+k)}{2}\left[\mathrm{erf}\left(\frac{vu-x}{2\sqrt{D'u}}\right)+\exp\left(\frac{vx}{D'}\right)\mathrm{erf}\left(\frac{vu+x}{2\sqrt{D'u}}\right)\right]_{u=\max(0,t-T)}^{u=t},$$

where we have made use of $v=(v_0/(1+k))$.

References

Bhatia, R. 2007 *Positive definite matrices.* Princeton series in applied mathematics. Princeton, NJ: Princeton University Press.

Crank, J. 1975 *Mathematics of diffusion*, 2nd edn. Oxford, UK: Oxford University Press.

Gardner, J. W., Covington, J. A., Koickal, T. J., Hamilton, A., Tan, S.-L. & Pearce, T. C. 2007 Towards an artificial human olfactory mucosa for improved odour classification. *Proc. R. Soc. A* **463**, 1713–1728. (doi:10.1098/rspa.2007.1844)

Golay, M. 1958 Theory of capillary columns. In *Gas Chromatography—Proc. 2nd Symp. on Gas Chromatography, Amsterdam, 19–23 May 1958* (ed. D. H. Desty), pp. 36–55. London, UK: Butterworth Press.

Kent, P. F., Mozell, M. M., Murphy, S. J. & Hornung, D. E. 1996 The interaction of imposed and inherent olfactory mucosal activity patterns and their composite representation in a mammalian species using voltage-sensitive dyes. *J. Neurosci.* **16**, 345–353.

Koickal, T. J., Hamilton, A., Tan, S. L., Covington, J. A., Gardner, J. W. & Pearce, T. C. 2007 Analog VLSI circuit implementation of an adaptive neuro-morphic olfaction chip. *IEEE Circ. Syst.* **54**, 60–73. (doi:10.1109/TCSI.2006.888677)

Llobet, E., Brezmes, J., Vilanova, X., Sueiras, J. E. & Correig, X. 1997 Qualitative and quantitative analysis of volatile organic compounds using transient and steady-state responses of a thick-film tin oxide gas sensor array. *Sensors Actuat. B: Chem.* **41**, 13–21. (doi:10.1016/S0925-4005(97)80272-9)

Marple, S. L. 1980 A new autoregressive spectrum analysis algorithm. *IEEE Trans. Acoust. Speech Signal Process.* **28**, 441–454. (doi:10.1109/TASSP.1980.1163429)

Pearce, T. C. & Sánchez-Montañés, M. A. 2003 Chemical sensor array optimization: geometric and theoretical approaches. In *Handbook of machine olfaction* (eds T. C. Pearce, S. S. Schiffman, H. T. Nagle & J. W. Gardner), pp. 347–375. Weinheim, Germany: Wiley-VCH.

Pearce, T. C., Schiffman, S. S., Nagle, H. T. & Gardner, J. W. 2003 *Handbook of machine olfaction.* Weinheim, Germany: Wiley-VCH.

Purnell, H. 1962 *Gas chromatography*, 1st edn. New York, NY: Wiley.

Sánchez-Montañés, M. A. & Pearce, T. C. 2001 Fisher information and optimal odour sensors. *Neurocomputing* **38**, 335–341. (doi:10.1016/S0925-2312(01)00364-2)

Schoenfeld, T. A. & Cleland, T. A. 2006 Anatomical contributions to odorant sampling and representation in rodents: zoning in on sniffing behavior. *Chem. Senses* **31**, 131–144. (doi:10.1093/chemse/bjj015)

Zamir, R. 1998 The Fisher information inequality via a data processing argument. *IEEE Trans. Inform. Theory* **44**, 1246–1250. (doi:10.1109/18.669301)